DOI: 10.14529/jsfi160206

Application of CUDA technology to calculation of ground states of few-body nuclei by Feynman's continual integrals method

Mikhail A. Naumenko[1], *Vyacheslav V. Samarin*[1,2]

The possibility of application of modern parallel computing solutions to speed up the calculations of ground states of few-body nuclei by Feynman's continual integrals method has been investigated. These calculations may sometimes require large computational time, particularly in the case of systems with many degrees of freedom. This paper presents the results of application of general-purpose computing on graphics processing units (GPGPU). The energy and the square modulus of the wave function of the ground states of several few-body nuclei have been calculated using NVIDIA CUDA technology. The results show that the use of GPGPU significantly increases the speed of calculations.

Keywords: NVIDIA CUDA, Feynman's continual integrals method, few-body nuclei.

Introduction

Low-energy reactions involving few-body nuclei [1] constitute a significant part of the studied nuclear reactions. Investigation of their collisions with other nuclei provides valuable information on the mechanisms of fusion and nucleon transfer reactions (*e.g.* [2]). Knowledge of the properties and the ground state wave functions of these nuclei is necessary for the theoretical description of reactions with their participation. The few-body problem in nuclear physics has been studied for a long time. For instance, calculations of ^{3}H and ^{3}He nuclei were performed in [3] based on the Faddeev equations. The expansion in hyperspherical functions (K-harmonics) [4] was used for calculations of ^{3}H nucleus in [5] and ^{4}He nucleus in [6]. In [7] the wave function of the three-body system was obtained using Gaussian basis and the numerical solution of the Hill-Wheeler integral equations.

Feynman's continual integrals method [8, 9] provides a more simple possibility for calculating the energy and the probability density for the ground state of the few-body system, because it does not require expansion of the wave function in a system of functions. This approach may be realized using the Monte-Carlo method with imaginary time and continuous variation of coordinates (*e.g.* [10–12]) or discrete coordinate lattice (*e.g.* within the nuclear lattice effective field theory [13, 14]). The possibility of application of the Monte-Carlo method with imaginary time and continuous variation of coordinates for calculation of energies of ground states of light nuclei up to ^{4}He was declared in [10, 11], but the power of computers available at that time did not allow obtaining reliable results since the statistics was very low. Even today, the authors usually either restrict themselves only to the calculation of energies of ground states of few-body nuclei [12, 13] or perform the more time-consuming calculation of wave functions with large lattice spacing (*e.g.* [14]), which is probably due to the lack of the computing power. In [15] calculations of both energies of ground states and wave functions were performed on the CPU with the statistics 10^5.

In this work an attempt is made to use modern parallel computing solutions to speed up the calculations of ground states of few-body nuclei by Feynman's continual integrals method. The algorithm allowing us to perform calculations directly on GPU was developed and implemented in C++ programming language. The energy and the square modulus of the wave function of the

[1]Joint Institute for Nuclear Research, Dubna, Russian Federation.
[2]Dubna State University, Dubna, Russian Federation.

ground states of several few-body nuclei have been calculated using NVIDIA CUDA technology [16–18]. The results show that the use of GPU is very effective for these calculations.

1. Theory

The energy E_0 and the square modulus of the wave function $|\Psi_0|^2$ of the ground state of a system of few particles may be calculated using continual (path) integrals introduced by Feynman [8, 9]. Feynman's integral

$$K\left(q,t;q_0,0\right)=\int Dq(t)\exp\left\{\frac{i}{\hbar}S\left[q(t')\right]\right\}=\left\langle q\left|\exp\left(-\frac{i}{\hbar}\hat{H}t\right)\right|q_0\right\rangle \tag{1}$$

is a propagator - the probability amplitude for the particle of mass m to travel from the point q_0 to the point q in time t. Here $S[q(t)]$ and $\hat{H}$ are the action and the Hamiltonian of the system, respectively, $Dq(t)$ is the integration measure [8, 9]. For the time-independent potential energy the transition to the imaginary (Euclidean) time $t=-i\tau$ gives the propagator $K_E\left(q,\tau;q_0,0\right)$

$$K_E\left(q,\tau;q_0,0\right)=\int D_Eq(\tau)\exp\left\{-\frac{1}{\hbar}S_E\left[q(\tau')\right]\right\} \tag{2}$$

with the Euclidean action

$$S_E\left[q(\tau')\right]=\int\limits_0^\tau d\tau'\left[\frac{m}{2}\left(\frac{dq}{d\tau'}\right)^2+V(q)\right]. \tag{3}$$

Integration over q with the periodic boundary condition $q=q_0$ allows us to find the energy E_0 of the ground state in the limit $\tau\to\infty$ [10, 11]

$$\int\limits_{-\infty}^{\infty}K_E\left(q,\tau;q,0\right)dq=\mathrm{Sp}\left[\exp\left(-\frac{\hat{H}\tau}{\hbar}\right)\right]=\sum_n\exp\left(-\frac{E_n\tau}{\hbar}\right)+\int\limits_{E_{\mathrm{cont}}}^{\infty}\exp\left(-\frac{E\tau}{\hbar}\right)g(E)dE, \tag{4}$$

$$\int\limits_{-\infty}^{\infty}K_E\left(q,\tau;q,0\right)dq\to\exp\left(-\frac{E_0\tau}{\hbar}\right),\tau\to\infty, \tag{5}$$

$$K_E\left(q,\tau;q,0\right)=\sum_n|\Psi_n(q)|^2\exp\left(-\frac{E_n\tau}{\hbar}\right)+\int\limits_{E_{\mathrm{cont}}}^{\infty}|\Psi_E(q)|^2\exp\left(-\frac{E\tau}{\hbar}\right)g(E)dE. \tag{6}$$

Here $g(E)$ is the density of states with the continuous spectrum $E\geq E_{\mathrm{cont}}$. For the system with a discrete spectrum and finite motion of particles the square modulus of the wave function of the ground state may also be found in the limit $\tau\to\infty$ [10, 11] together with the energy E_0

$$\hbar\ln K_E\left(q,\tau;q,0\right)\to\hbar\ln|\Psi_0(q)|^2-E_0\tau,\tau\to\infty, \tag{7}$$

$$K_E\left(q,\tau;q,0\right)\to|\Psi_0(q)|^2\exp\left(-\frac{E_0\tau}{\hbar}\right),\tau\to\infty. \tag{8}$$

The equation (7) may be used to find the energy E_0 as the slope of the linear part of the curve $\hbar\ln K_E\left(q,\tau;q,0\right)$ calculated for several increasing values of τ. The equation (8) may be used to find the square modulus of the wave function of the ground state $|\Psi_0(q)|^2$ in all points q of

the necessary region by calculating $K_E(q,\tau;q,0)$ at the fixed time τ corresponding to the linear part of the curve $\hbar \ln K_E(q,\tau;q,0)$.

Outside of the classically allowed region the square modulus of the wave function $|\Psi_0(q)|^2$ of the ground state with $E < E_{\text{cont}}$ may be significantly smaller than $|\Psi_E(q)|^2$ for the states with the continuous spectrum $E \geq E_{\text{cont}}$. The ground state term in the formula (6) will not dominate despite the much more rapid decrease of the exponential factors $\exp(-E\tau/\hbar) \ll \exp(-E_0\tau/\hbar), E > E_0$. Therefore, in this case the formulas (7), (8) are in general applicable only for the region not far beyond the classically allowed ground state region.

Such situation may occur in the description of bound states of few-particle systems (*e.g.* two protons and a neutron) when the existence of bound states of some of them (*e.g.* proton plus neutron) is possible.

The contribution of states with the continuum spectrum may be eliminated by introducing infinitely high walls in the potential energy located about the range of the nuclear forces beyond the classically allowed region. Introduction of the boundary condition $\Psi_0(q) = 0$ at these walls will not have a significant effect on the energy E_0 and $|\Psi_0(q)|^2$ far away from the walls.

Feynman's continual integral (2) may be represented as the limit of the multiple integral

$$K(q,\tau;q_0,0) = \lim_{\substack{N\to\infty \\ N\Delta\tau=\tau}} \int\cdots\int \exp\left\{-\frac{1}{\hbar}\sum_{k=1}^{N}\left[\frac{m(q_k-q_{k-1})^2}{2\Delta\tau} - \frac{V(q_k)+V(q_{k-1})}{2}\Delta\tau\right]\right\}\times \\ \times C^N dq_1 dq_2 \ldots dq_{N-1}, \tag{9}$$

where

$$q_k = q(\tau_k), \tau_k = k\Delta\tau, k = \overline{0,N}, q_N = q, C = \left(\frac{m}{2\pi\hbar\Delta\tau}\right)^{1/2}. \tag{10}$$

Here $(N-1)$-fold integral corresponds to averaging over the "path" of the particle as a broken line in the plane (q,τ) with the vertices $(q_k,\tau_k), k = \overline{1,N-1}$.

For the approximate calculation of the continual integral (9) the continuous axis τ is replaced with the grid $\tau = \tau_k = k\Delta\tau, k = \overline{0,N}, N \geq 2$ with the step $\Delta\tau$ and the Euclidean propagator of a free particle $K_E^{(0)}(q,\tau;q_0,0)$ is separated [9, 10]

$$K_E(q,\tau;q_0,0) \approx K_E^{(0)}(q,\tau;q_0,0)\left\langle \exp\left[-\frac{\Delta\tau}{2\hbar}\sum_{k=1}^{N}(V(q_k)+V(q_{k-1}))\right]\right\rangle, \tag{11}$$

$$K_E^{(0)}(q,\tau;q_0,0) = \left(\frac{m}{2\pi\hbar\tau}\right)^{1/2}\exp\left[-\frac{m(q-q_0)^2}{2\hbar\tau}\right]. \tag{12}$$

Requiring $q_N = q_0$, we obtain

$$K_E(q_0,\tau;q_0,0) \approx K_E^{(0)}(q_0,\tau;q_0,0)\left\langle \exp\left[-\frac{\Delta\tau}{\hbar}\sum_{k=1}^{N}V(q_k)\right]\right\rangle, \tag{13}$$

$$K_E^{(0)}(q_0,\tau;q_0,0) = \left(\frac{m}{2\pi\hbar\tau}\right)^{1/2}. \tag{14}$$

Here and below the angle brackets mean averaging of the values of the quantity F

$$F = \exp\left[-\frac{\Delta\tau}{\hbar}\sum_{k=1}^{N}V(q_k)\right] \tag{15}$$

over random trajectories, *i.e.* over $(N-1)$-dimensional vectors $Q = \{q_1, \ldots, q_{N-1}\}$ with the distribution law $W(q_0; q_1, \ldots, q_{N-1}; q_N = q_0)$

$$W(q_0; q_1, \ldots, q_{N-1}; q_N = q_0) = C^{N-1} N^{1/2} \exp\left[-\frac{m}{2\hbar\Delta\tau}\sum_{k=1}^{N}(q_k - q_{k-1})^2\right]. \tag{16}$$

This averaging may be calculated using the Monte Carlo method [19]

$$\langle F\rangle = \frac{1}{n}\sum_{i=1}^{n} F_i, \tag{17}$$

where n is the total number of random trajectories, $n \sim 10^5$ - 10^7.

The standard algorithm for simulation of the random vector consists in a sequential choice of the values of its components from the conditional distributions $W_1(q_1)$, $W_2(q_2|q_1)$, $W_3(q_3|q_1, q_2)$, ..., $W_{N-1}(q_{N-1}|q_1, q_2, \ldots, q_{N-2})$ [20]. Here $W_k(q_k|q_1, q_2, \ldots, q_{k-1})$ is the probability density for the values of the quantity q_k given the values of quantities $q_1, q_2, \ldots, q_{k-1}$. For example, for k=1

$$\begin{aligned} W(q_1) = \int dq_2 \ldots \int dq_{N-1} W(q_0; q_1, q_2, \ldots q_{N-1}; q_N = q_0) = \\ = \frac{1}{\sqrt{2\pi\sigma_1}} \exp\left\{-\frac{1}{2\sigma_1}\left[(\mathrm{M}q_1 - q_1)^2\right]\right\}, \end{aligned} \tag{18}$$

$$\sigma_1 = \frac{\hbar\Delta\tau}{m}\left(1 - \frac{1}{N}\right), \mathrm{M}q_1 = q_0. \tag{19}$$

In the case of k=2

$$\begin{aligned} W_2(q_2|q_1) = \int dq_3 \ldots \int dq_{N-1} W(q_0; q_1, q_2, q_3, \ldots q_{N-1}; q_N = q_0) = \\ = \frac{1}{\sqrt{2\pi\sigma_2}} \exp\left\{-\frac{1}{2\sigma_2}\left[(\mathrm{M}q_2 - q_2)^2\right]\right\} \frac{1}{\sqrt{2\pi\sigma_1}} \exp\left\{-\frac{1}{2\sigma_1}\left[(\mathrm{M}q_1 - q_1)^2\right]\right\}, \end{aligned} \tag{20}$$

$$\sigma_2 = \frac{\hbar\Delta\tau}{m}\left(1 - \frac{1}{N-1}\right), \mathrm{M}q_2 = \left(1 - \frac{1}{N-1}\right) q_1 + \frac{1}{N-1} q_0. \tag{21}$$

Finally, in the general case

$$\begin{aligned} W_k(q_k|q_1, q_2, \ldots, q_{k-1}) = \int dq_{k+1} \ldots \int dq_{N-1} W(q_0; q_1, q_2, q_3, \ldots, q_{N-1}; q_N = q_0) = \\ = \frac{1}{\sqrt{2\pi\sigma_k}} \exp\left\{-\frac{1}{2\sigma_2}\left[(\mathrm{M}q_k - q_k)^2\right]\right\} \ldots \frac{1}{\sqrt{2\pi\sigma_1}} \exp\left\{-\frac{1}{2\sigma_1}\left[(\mathrm{M}q_1 - q_1)^2\right]\right\}, \end{aligned} \tag{22}$$

$$\sigma_k = \frac{\hbar\Delta\tau}{m}\left(1 - \frac{1}{N-k+1}\right), \mathrm{M}q_k = \left(1 - \frac{1}{N-k+1}\right) q_{k-1} + \frac{1}{N-k+1} q_0. \tag{23}$$

Introducing the variable A_k

$$A_k = (N-k+1)^{-1} \tag{24}$$

we obtain that the quantity q_k is normally distributed with the mean value $\mathrm{M}q_k$, variance D_k and standard deviation $\sigma_k = \sqrt{D_k}$ [15]

$$\mathrm{M}q_k = (1 - A_k) q_{k-1} + A_k q_0, \tag{25}$$

$$D_k = (1 - A_k) \hbar\Delta\tau/m, \tag{26}$$

$$\sigma_k = [(1 - A_k)\hbar\Delta\tau/m]^{1/2}. \tag{27}$$

In the simulation the next point q_k of the trajectory is calculated by the formula

$$q_k = \mathrm{M}q_k + \zeta_k\sigma_k, k = \overline{1, N-1}, \tag{28}$$

where ζ_k is a normally distributed random variable with zero mean and unity variance. Sample one-dimensional random trajectories for low $N = 6$ and large $N = 1200$ numbers of time steps are shown in fig. 1a and fig. 1b, respectively.

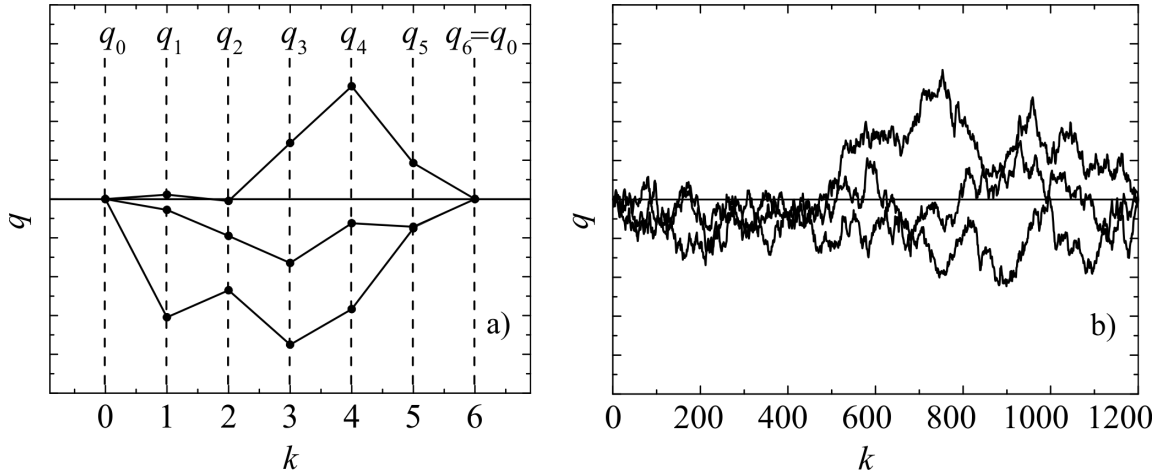

Figure 1. Sample one-dimensional random trajectories for low $N = 6$ (a) and large $N = 1200$ (b) numbers of time steps

For large values of τ random trajectories may reach the region where the probability density for the states with continuum spectrum is substantially larger than the probability density for the ground state, which may lead to a deviation from the asymptotic behavior (7), (8) and the growth of the error. Therefore, the formulas (7), (8) are only applicable for the not very large values of τ.

For convenience of calculations in the scale of nuclear forces we introduce dimensionless variables

$$\tilde{q} = q/x_0, \tilde{\tau} = \tau/t_0, \Delta\tilde{\tau} = \Delta\tau/t_0, \tilde{V} = V(q)/\varepsilon_0, \tilde{E}_0 = E_0/\varepsilon_0, \tilde{m} = m/m_0, \tag{29}$$

where $x_0 = 1$ fm, $\varepsilon_0 = 1$ MeV, m_0 is the neutron mass, $t_0 = m_0 x_0^2/\hbar \approx 1.57 \cdot 10^{-23}$ sec, $b_0 = t_0\varepsilon_0/\hbar \approx 0.02412$. The expressions (7), (8), (13), (16), (25) - (27) may now be represented as

$$\tilde{K}_E(\tilde{q}_0, \tilde{\tau}; \tilde{q}_0, 0) \approx x_0^{-1}\left(\frac{\tilde{m}}{2\pi\tilde{\tau}}\right)^{1/2}\left\langle \exp\left[-b_0\Delta\tilde{\tau}\sum_{k=1}^{N}\tilde{V}(\tilde{q}_k)\right]\right\rangle, \tag{30}$$

$$\tilde{D}_k = \tilde{\sigma}_k^2, \tilde{q}_k = \mathrm{M}\tilde{q}_k + \zeta_k\tilde{\sigma}_k, \tilde{\sigma}_k = x_0[(1 - A_k)\Delta\tilde{\tau}/\tilde{m}]^{1/2}, \tag{31}$$

$$W(\tilde{q}_0; \tilde{q}_1, \ldots, \tilde{q}_{N-1}; \tilde{q}_N) = C^{N-1}N^{1/2}\exp\left[-\frac{1}{2\Delta\tilde{\tau}}\sum_{k=1}^{N}(\tilde{q}_k - \tilde{q}_{k-1})^2\right], \tag{32}$$

$$\frac{1}{b_0}\ln\tilde{K}_E(\tilde{q}, \tilde{\tau}; \tilde{q}, 0) \to \frac{1}{b_0}\ln|\Psi_0(\tilde{q})|^2 - \tilde{E}_0\tilde{\tau}, \tilde{\tau} \to \infty, \tag{33}$$

$$\tilde{K}_E(\tilde{q}, \tilde{\tau}; \tilde{q}, 0) \to |\Psi_0(\tilde{q})|^2\exp\left(-b_0\tilde{E}_0\tilde{\tau}\right), \tilde{\tau} \to \infty. \tag{34}$$

The above formulas are naturally generalized to a larger number of degrees of freedom and few particles including identical ones. The nuclei ^{3}H, ^{3}He and ^{4}He contain no more than two identical fermions (protons and/or neutrons with opposite spins), which ensures that the Pauli Exclusion Principle is satisfied for their ground states. The nucleon identity requires symmetrization of trajectories [11], which is achieved by choosing the Jacobi coordinates in such a way that vectors connect two identical fermions (see below).

It should be noted that the calculation of multiple integrals required to find the multidimensional probability density $|\Psi_0|^2$ by Feynman's continual integrals method continues to be a challenging task. However, the analysis of the properties of $|\Psi_0|^2$ allows us to choose analytical approximations of $|\Psi_0|^2$, *e.g.* as the product of the Gaussian type exponentials. The obtained approximations may be used in dynamic calculations. The application of the formula (7) in a single point in the multidimensional space allows us to find the approximate value of the energy of the ground state.

To reduce the number of degrees of freedom and multiplicity of integrals in the formula (11) the calculation should be performed in the center of mass system using the Jacobi coordinates [4, 9].

For a system of two particles (^{2}H nucleus)

$$\vec{R} = \vec{r}_2 - \vec{r}_1, \tag{35}$$

where $\vec{r}_1$ and $\vec{r}_2$ are the radius vectors of a proton and a neutron, respectively.

For a system of three particles, two of which are identical (2 neutrons or 2 protons in ^{3}H and ^{3}He nuclei, respectively)

$$\vec{R} = \vec{r}_2 - \vec{r}_1, \vec{r} = \vec{r}_3 - \frac{1}{2}\left(\vec{r}_1 + \vec{r}_2\right). \tag{36}$$

In the case of ^{3}H nucleus $\vec{r}_3$ is the radius vector of a proton, $\vec{r}_1$ and $\vec{r}_2$ are the radius vectors of neutrons. In the case of ^{3}He nucleus $\vec{r}_3$ is the radius vector of a neutron, $\vec{r}_1$ and $\vec{r}_2$ are the radius vectors of protons.

For a system of four particles consisting of two pairs of identical particles (2 protons and 2 neutrons in ^{4}He nucleus)

$$\vec{R}_1 = \vec{r}_2 - \vec{r}_1, \vec{R}_2 = \vec{r}_4 - \vec{r}_3, \vec{r} = \frac{1}{2}\left(\vec{r}_3 + \vec{r}_4\right) - \frac{1}{2}\left(\vec{r}_1 + \vec{r}_2\right), \tag{37}$$

where $\vec{r}_1$ and $\vec{r}_2$ are the radius vectors of protons, $\vec{r}_3$ and $\vec{r}_4$ are the radius vectors of neutrons.

The energy of the ground states of bound nuclei is negative $E_0 < 0$, whereas the binding energy E_b (the energy required to disassemble a nucleus into separate nucleons) is positive, $E_b = -E_0 > 0$.

In the calculation of the propagator $K\left(q, \tau; q_0, 0\right)$ for the nuclei ^{2}H, ^{3}H, ^{3}He, ^{4}He neutron-proton $V_{n-p}(r)$, neutron-neutron $V_{n-n}(r)$ and proton-proton $V_{p-p}(r)$ two-body strong interaction potentials have been used. The dependence of the nucleon-nucleon strong interaction with a repulsive core on the distance r was approximated by a combination of Gaussian type exponentials similar to the M3Y potential [21, 22]

$$V_{n-n}(r) \equiv V_{p-p}(r) = \sum_{k=1}^{3} u_k \exp\left(-r^2/b_k^2\right), \tag{38}$$

$$V_{n-p}(r) = \eta V_{n-n}(r). \tag{39}$$

The total interaction potential $V(r) \equiv V_{n-n}(r)$ for two neutrons, $V(r) \equiv V_{n-p}(r)$ for a neutron and a proton, $V(r) \equiv V_{p-p}(r) + e^2/r$ for two protons (here the last term represents the Coulomb part of the potential). The values of the parameters $u_1 = 500$ MeV, $u_2 = -102$ MeV, $u_3 = 2$ MeV, $b_1 = 0.606$ fm, $b_2 = 1.437$ fm, $b_3 = 3.03$ fm and $\eta = 1.2$ provide the absence of bound states of two identical nucleons as well as the approximate equality of the energy $E_b = -E_0$ found from the formula (33) to the experimental values of the binding energies for the nuclei ^{2}H, ^{3}H, ^{3}He, ^{4}He taken from the knowledge base [23] (the comparison is given in tab. 1 below). The plots of the total interaction potential $V(r)$ for two neutrons, a neutron and a proton, and two protons are shown in fig. 2.

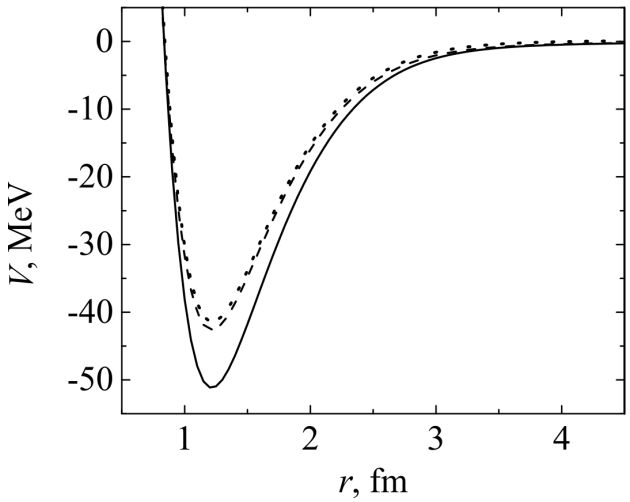

Figure 2. The neutron-proton (solid line), neutron-neutron (dashed line), and proton-proton (dotted line) total interaction potentials $V(r)$

2. Implementation

The Monte Carlo algorithm for numerical calculations was developed and implemented in C++ programming language using NVIDIA CUDA technology. The code samples are not included in the publication, because the algorithm is described in detail in mathematical, physical and implementation aspects, in contrast to *e.g.* [10, 11]. The paper itself is to a great extent the description of the integration method which does not require the use of any additional integration libraries. The detailed description of the algorithm provided allows anyone to easily implement it.

The calculation included 3 steps:

1. $\tilde{K}_E(\tilde{q}, \tilde{\tau}; \tilde{q}, 0)$ was calculated in a set of multidimensional points $\tilde{q}$ (*e.g.* $\left\{\vec{R}; \vec{r}\right\}$ for ^{3}H and ^{3}He nuclei) and the maximum of $\tilde{K}_E(\tilde{q}, \tilde{\tau}; \tilde{q}, 0)$ (*i.e.* $|\Psi_0|^2$) was found.
2. The point $\tilde{q}_0$ corresponding to the obtained maximum was fixed, $\tilde{K}_E(\tilde{q}_0, \tilde{\tau}; \tilde{q}_0, 0)$ was calculated for several increasing values of $\tilde{\tau}$ and the linear region of $\ln \tilde{K}_E(\tilde{q}_0, \tilde{\tau}; \tilde{q}_0, 0)$ was found for calculation of the energy $\tilde{E}_0$ using formula (33).
3. The time $\tilde{\tau}_{\text{lin}}$ corresponding to the beginning of the obtained linear region was fixed and $\tilde{K}_E(\tilde{q}_0, \tilde{\tau}_{\text{lin}}; \tilde{q}_0, 0)$ (*i.e.* $|\Psi_0|^2$) was calculated in all points of the necessary region using formula (34).

The calculation of $\tilde{K}_E(\tilde{q}, \tilde{\tau}; \tilde{q}, 0)$ for the fixed $\tilde{\tau}$ was performed by parallel calculation of exponentials F

$$F = \exp\left[-b_0 \Delta\tilde{\tau} \sum_{k=1}^{N} \tilde{V}(\tilde{q}_k)\right] \tag{40}$$

for every trajectory in a given kernel launch, where $N = \tilde{\tau}/\Delta\tilde{\tau}$.

The principal scheme of the calculation of the ground state energy is shown in fig. 3. The calculation of the propagator (30) is performed using L sequential launches of the kernel. Each kernel launch simulates n random trajectories in the space evolving from the Euclidean time $\tilde{\tau} = 0$ to $\tilde{\tau}_j$, where $j = \overline{1, L}$ (see fig. 1). All trajectories with $N_j = \tilde{\tau}_j/\Delta\tilde{\tau}$ time steps start at the same point $q^{(0)}$ in the space and in the moment $\tilde{\tau}_j$ return back to the same point $q^{(0)}$ according to the probability distribution described above.

The choice of the initial point $q^{(0)}$ is arbitrary for $\tilde{\tau} \to \infty$, but it is clear that for the finite values of $\tilde{\tau}$ available in calculations the point $q^{(0)}$ must be located within the region Ω the integral over which of the square modulus of the normalized ground state wave function is close enough to unity

$$\int_{\Omega} |\Psi_0(q)|^2 dq \approx 1 \tag{41}$$

in order to ensure less number of time steps in the calculation and obtain more accurate results.

All threads in a given kernel launch finish at approximately the same time, which makes the scheme quite effective in spite of the possible delays associated with the kernel launch overhead. Besides, the typical number of kernel launches L required for the calculation of the ground state energy usually does not exceed 100.

Starting from the certain time $\tilde{\tau}_{\text{lin}}$ the obtained values of the logarithm of the propagator $b_0^{-1} \ln \tilde{K}_E$ (30) tend to lie on the straight line, the slope of which gives the value of the ground state energy. The time $\tilde{\tau}_{\text{lin}}$ is then used in the calculation of the square modulus of the wave function.

The principal scheme of the calculation of the square modulus of the wave function is shown in fig. 4. Similarly, the calculation is performed using M sequential launches of the kernel. Each kernel launch simulates n random trajectories in the space evolving from the Euclidean time $\tilde{\tau} = 0$ to the time $\tilde{\tau}_{\text{lin}}$ determined in the calculation of the ground state energy. All trajectories start at the same point $q^{(s)}$ in the space and in the moment $\tilde{\tau}_{\text{lin}}$ return back to the same point $q^{(s)}$ according to the probability distribution described above. Here $s = \overline{1, M}$, where M is the total number of points in the space in which the square modulus of the wave function must be calculated.

One of the benefits of the approach is that the calculation may be easily resumed at a later time. For example, initially the square modulus of the wave function may be calculated with a large space step to obtain the general features of the probability distribution, and later new intermediate points are calculated and combined with those calculated previously. This may be very useful because the calculation of the square modulus of the wave function is generally much more time-consuming since it requires calculation in many points in the multidimensional space.

An important feature of the algorithm allowing effective use of graphic processors is low consumption of memory during the calculation because it is not necessary to prepare a grid of values and store it in the memory.

To obtain normally distributed random numbers the cuRAND random number generator was used. According to the recommendations of the cuRAND developers each experiment was

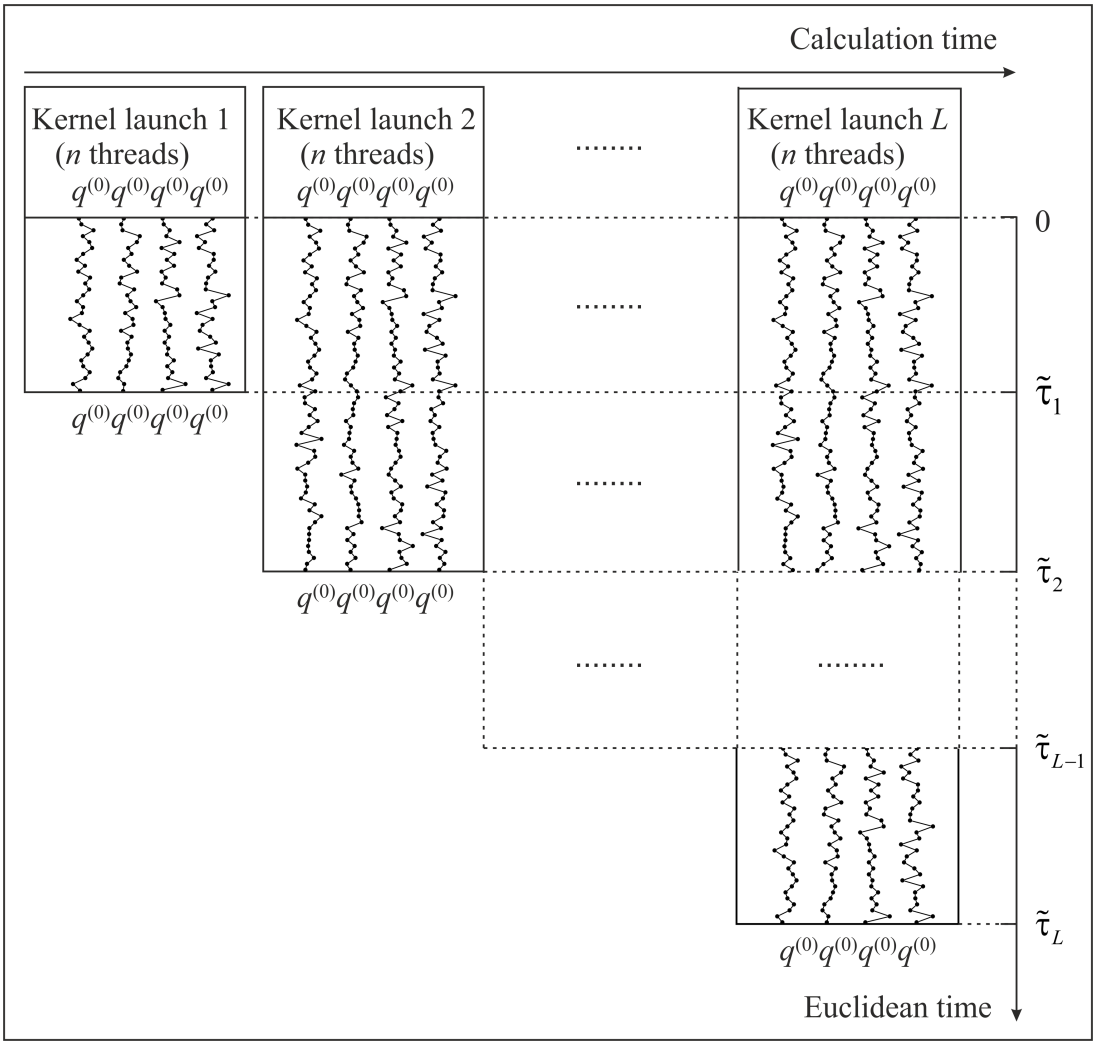

Figure 3. The scheme of calculation of the ground state energy E_0 using formula (33)

assigned a unique seed. Within the experiment, each thread of computation was assigned a unique sequence number. All threads between kernel launches were given the same seed, and the sequence numbers were assigned in a monotonically increasing way.

3. Results and discussion

Calculations were performed on the NVIDIA Tesla K40 accelerator installed within the heterogeneous cluster [24] of the Laboratory of Information Technologies, Joint Institute for Nuclear Research, Dubna. The code was compiled with NVIDIA CUDA version 7.5 for architecture version 3.5. Calculations were performed with single precision. The Euclidean time step $\Delta\tilde{\tau} = 0.01$ was used. Additionally, NVIDIA GeForce 9800 GT accelerator was used for debugging and testing purposes.

The dependence of logarithm of the propagator $b_0^{-1} \ln \tilde{K}_E$ on the Euclidean time $\tilde{\tau}$ is shown in fig. 5 for nuclei ^{2}H (a), ^{3}H (b), ^{3}He (c) and ^{4}He (d). Different symbols correspond to different statistics n: empty circles (10^5), filled circles (10^6, $5{\cdot}10^6$, 10^7).

The behavior of the curves may be easily explained if we note that in all these cases only the energy of the ground state is negative and therefore only the first term in (6) increases with

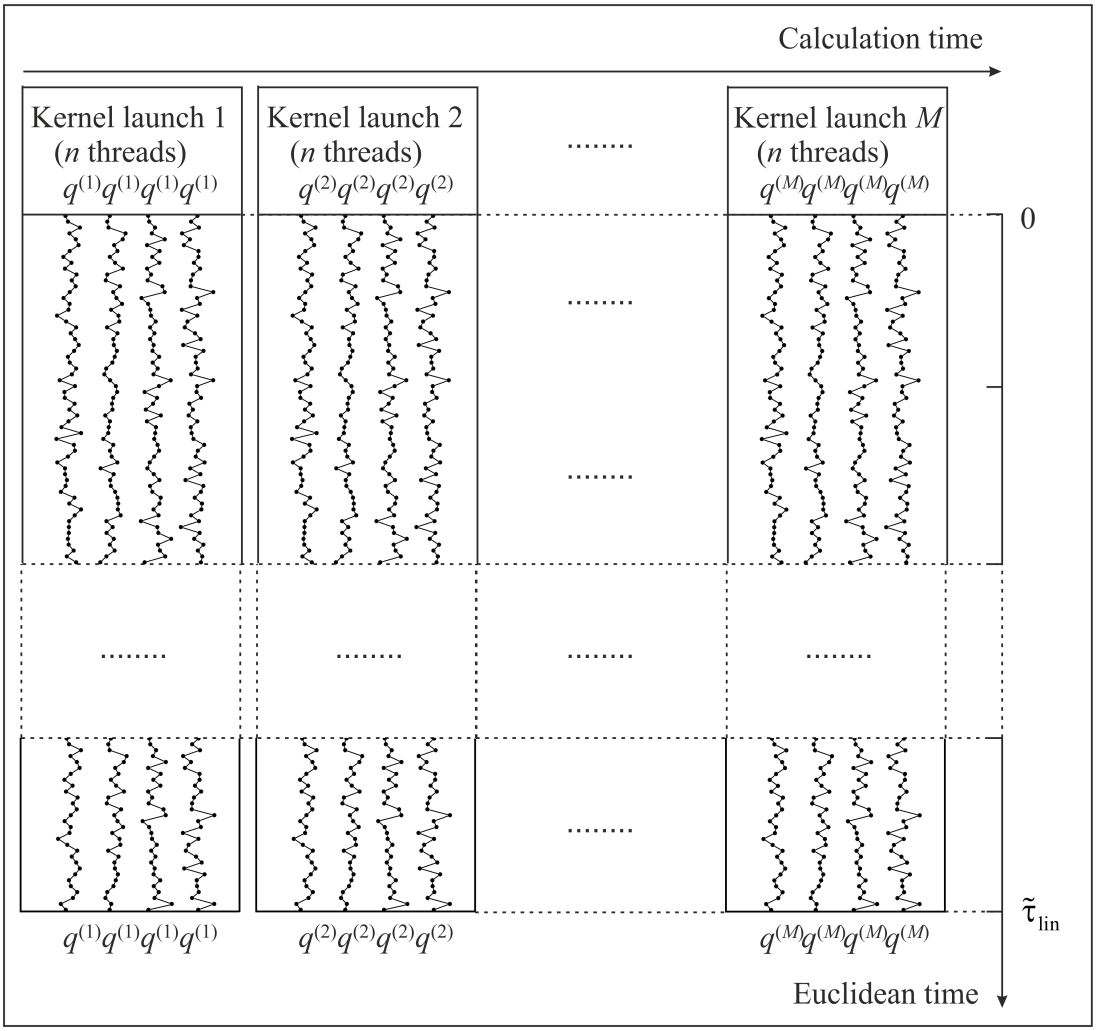

Figure 4. The scheme of calculation of the square modulus of the wave function $|\Psi_0(q)|^2$ using formula (34)

the increase of $\tilde{\tau}$, whereas the energies of the excited states are positive and hence the other terms in (6) decrease with the increase of $\tilde{\tau}$.

The results of linear fitting of the straight parts of the curves are shown in fig. 5e-h. According to the formula (33) the slope of the linear regression equals the energy of the ground state E_0. The obtained theoretical binding energies $E_b = -E_0$ are listed in tab. 1 together with the experimental values taken from the knowledge base [23]. It is clear that the theoretical values are close enough to the experimental ones, though obtaining good agreement was not the goal. The observed difference between the calculated binding energies of ^{3}H and ^{3}He is also in agreement with the experimental values.

The comparison of the square modulus of the wave function for ^{2}H calculated on GPU using NVIDIA CUDA technology within Feynman's continual integrals method and the square modulus of the wave function calculated on CPU within the shell model is shown in fig. 6a. The same potentials (38), (39) were used. Good agreement between the curves confirms that the code based on Feynman's continual integrals method using NVIDIA CUDA technology provides correct results.

It should be mentioned that the wave function cannot be measured directly, though the charge radii and charge distributions obtained from experiments may provide some information

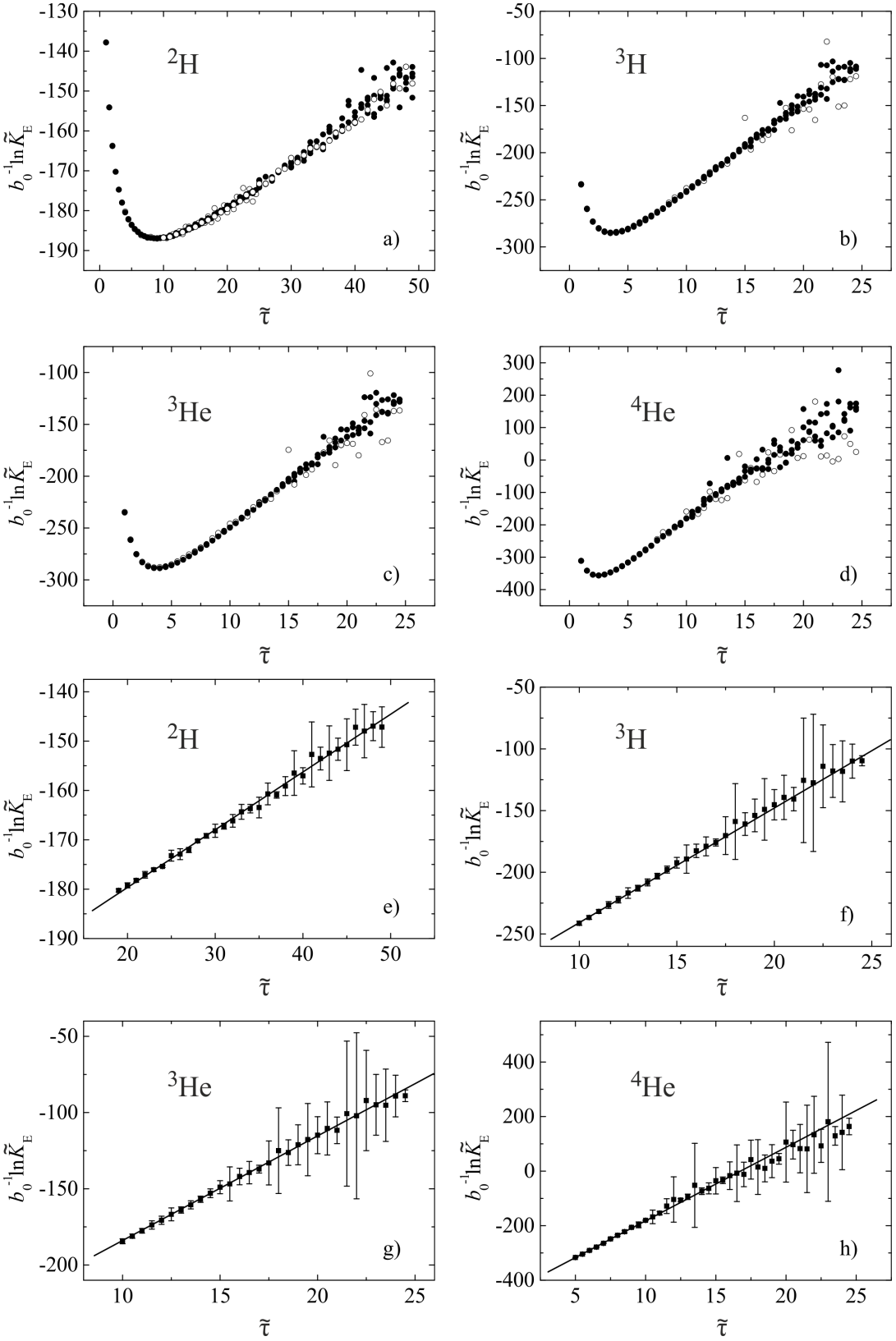

Figure 5. The dependence of the logarithm of the propagator $b_0^{-1}\ln\tilde{K}_E$ on the Euclidean time $\tilde{\tau}$ for ^{2}H (a), ^{3}H (b), ^{3}He (c) and ^{4}He (d). Lines are the results of linear fitting of the data lying on the straight parts of the curves for ^{2}H (e), ^{3}H (f), ^{3}He (g) and ^{4}He (h). Different symbols correspond to different statistics n: empty circles (10^5), filled circles (10^6, $5{\cdot}10^6$, 10^7)

Table 1. Comparison of theoretical and experimental binding energies for the ground states of the studied nuclei

Atomic nucleus	Theoretical value, MeV	Experimental value, MeV
^{2}H	1.17 ± 1	2.225
^{3}H	9.29 ± 1	8.482
^{3}He	6.86 ± 1	7.718
^{4}He	26.95 ± 1	28.296

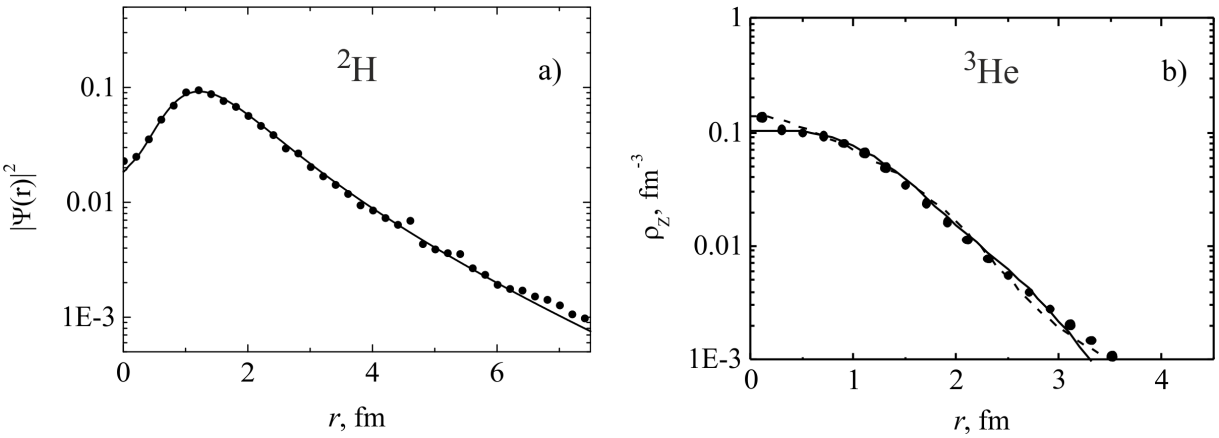

Figure 6. (a) The square modulus of the wave function for ^{2}H calculated on GPU using NVIDIA CUDA technology within Feynman's continual integrals method (circles) compared with the square modulus of the wave function calculated on CPU within the shell model (line); r is the distance between the proton and the neutron. (b) The theoretical charge distribution for ^{3}He (circles) compared with experimental data taken from taken from the knowledge base [23] (lines)

on its behavior. To compare the results of calculations with the experimental charge radii and charge distributions the wave function must be integrated.

The probability density distribution $\left|\Psi_0\left(\vec{R};\vec{r}\right)\right|^2$ for the configurations of ^{3}He nucleus ($p+p+n$) with the angle $\theta = 0°$, $45°$, $90°$ between the vectors $\vec{R}$ and $\vec{r}$ is shown in logarithmic scale in fig. 7a,b,c, respectively, together with the potential energy surface (linear scale, lines). The vectors in the Jacobi coordinates are shown in fig. 7d.

The theoretical charge distribution for ^{3}He obtained by integration of the wave function is compared with experimental data taken from taken from the knowledge base [23] in fig. 6b. As can be seen, the agreement is very good. The obtained theoretical charge radius $\left\langle R_{ch}^2\right\rangle^{1/2} = 1.94$ fm is also very close to the experimental value 1.9664 ± 0.0023 fm.

The probability density distribution for the symmetric tetrahedral configuration of four nucleons in the nucleus ^{4}He

$$\left|\Psi_0\left(\vec{R}_1;\vec{r};\vec{R}_2\right)\right|^2 = \left|\Psi_0\left(R_{1x},0,0;0,0,r_z;0,R_{2y}=R_{1x},0\right)\right|^2, \tag{42}$$

$$\vec{R}_1 \perp \vec{r} \perp \vec{R}_2,\ \left|\vec{R}_1\right| = \left|\vec{R}_2\right|, \vec{R}_1 = \left(R_{1x},0,0\right), \vec{r} = \left(0,0,r_z\right), \vec{R}_2 = \left(0,R_{2y}=R_{1x},0\right) \tag{43}$$

is shown in logarithmic scale in fig. 7e together with the potential energy surface (linear scale, lines). The vectors in the Jacobi coordinates are shown in fig. 7f.

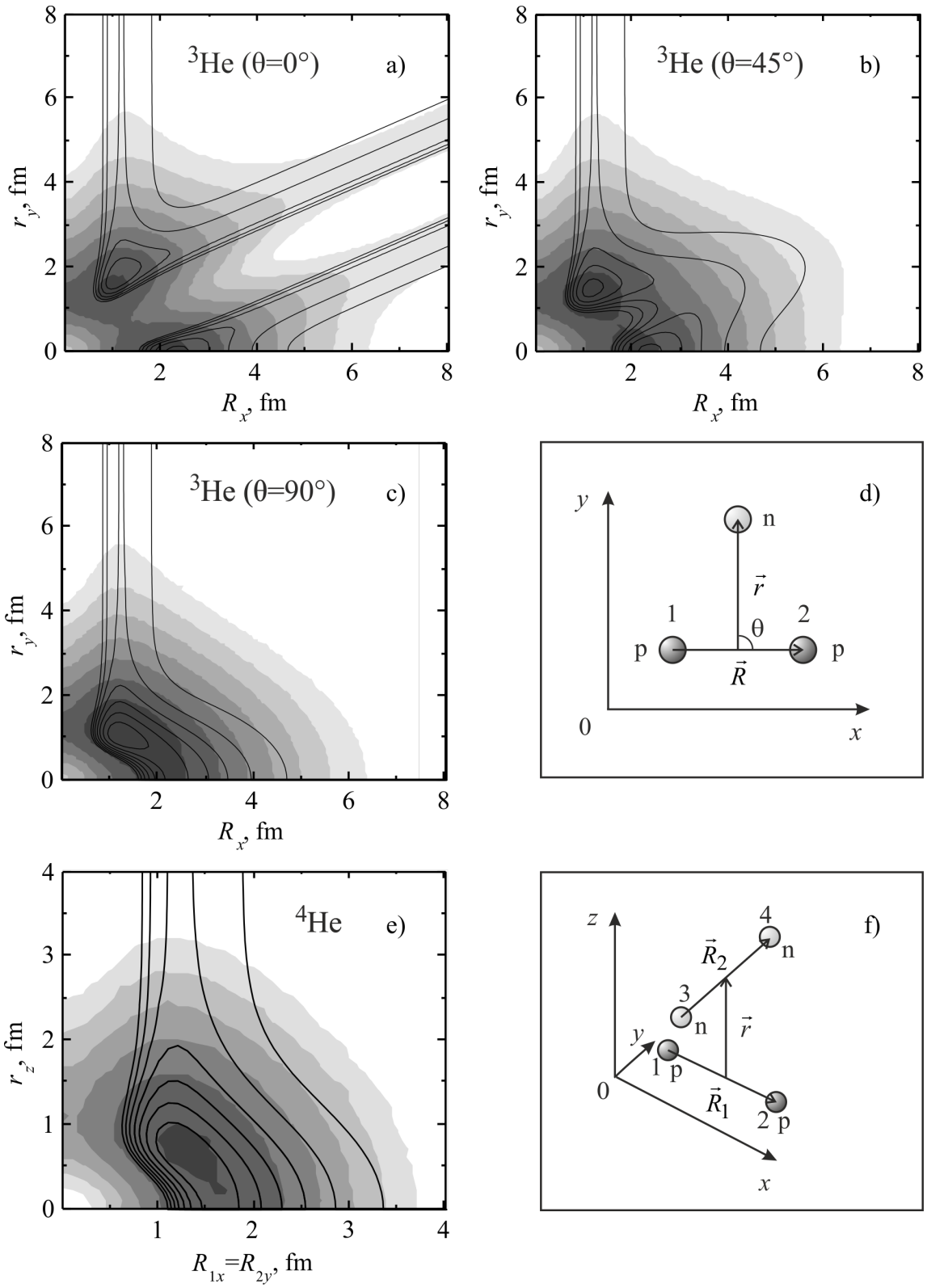

Figure 7. The probability density for the configurations of ^{3}He with $\theta = 0°$ (a), 45° (b), 90° (c) and the vectors in the Jacobi coordinates (d). The probability density for the configuration of ^{4}He symmetric with respect to the positions of protons and neutrons (e) and the vectors in the Jacobi coordinates (f)

Note also that the presence of the repulsive core in the nucleon-nucleon interaction reduces the probability of finding nucleons in the center of mass of the system for the considered sym-

metric configurations. This should lead to a smoother increase in the concentration of nucleons and the density of electric charge when approaching the center of the nucleus.

The analysis of the properties of $|\Psi_0|^2$ obtained by Feynman's continual integrals method was used to refine the shell model for light nuclei [15].

The code implementing Feynman's continual integrals method was initially written for CPU. The comparison of the calculation time of the ground state energy for ^{3}He using Intel Core i5 3470 (double precision) and NVIDIA Tesla K40 (single precision) with different statistics is shown in tab. 2. Even taking into account that the code for CPU used only 1 thread, double precision and a different random number generator, the time difference is impressive. This fact allows us to increase the statistics and the accuracy of calculations in the case of using NVIDIA CUDA technology.

Table 2. Comparison of the calculation time of the ground state energy for ^{3}He nucleus

Statistics, n	Intel Core i5 3470 (1 thread, double precision), sec	NVIDIA Tesla K40 (single precision), sec	Performance gain, times
10^5	∼1854	∼8	∼232
10^6	∼18377	∼47	∼391
$5{\cdot}10^6$	-	∼221	-
10^7	-	∼439	-

The comparison of the calculation time of the square modulus of the wave function $\left|\Psi_0\left(\vec{R};\vec{r}\right)\right|^2$ for the ground state of ^{3}He using Intel Core i5 3470 and NVIDIA Tesla K40 with the statistics 10^6 for every point in the space $\left\{\vec{R};\vec{r}\right\}$ and the total number of points 43200 is shown in tab. 3. The value ∼177 days for CPU is an estimation based on the performance gain in the calculation of the ground state energy. It is evident that beside the performance gain the use of NVIDIA CUDA technology may allow us to reduce the space step in the calculation of the wave functions, as well as greatly simplify the process of debugging and testing, and in certain cases it may even enable calculations impossible before.

Table 3. Comparison of the calculation time of the square modulus of the wave function for the ground state of ^{3}He nucleus

Statistics, n	Intel Core i5 3470 (1 thread, double precision, estimation)	NVIDIA Tesla K40 (single precision)
10^6	∼177 days	∼11 hours

4. Conclusion

In this work an attempt is made to use modern parallel computing solutions to speed up the calculations of ground states of few-body nuclei by Feynman's continual integrals method. The algorithm allowing us to perform calculations directly on GPU was developed and implemented in C++ programming language. The method was applied to the nuclei consisting of nucleons, but it may also be applied to the calculation of cluster nuclei. The energy and the square modulus of the wave function of the ground states of several few-body nuclei have been calculated by

Feynman's continual integrals method using NVIDIA CUDA technology. The comparison with the square modulus of the wave function for ^{2}H calculated on CPU within the shell model was performed to confirm the correctness of the calculations. The obtained values of the theoretical binding energies are close enough to the experimental values. The theoretical charge radius and charge distribution for ^{3}He nucleus are also in good agreement with the experimental data. The results show that the use of GPGPU significantly increases the speed of calculations. This allows us to increase the statistics and the accuracy of calculations as well as reduce the space step in calculations of wave functions. It also greatly simplifies the process of debugging and testing. In certain cases the use of NVIDIA CUDA enables calculations impossible before.

The work was supported by grant 15-07-07673-a of the Russian Foundation for Basic Research (RFBR).

The paper is recommended for publication by the Program Committee of the "Parallel computational technologies (PCT) 2016" International Scientific Conference

References

1. Penionzhkevich Yu.E. Reactions Involving Loosely Bound Cluster Nuclei: Heavy Ions and New Technologies // Phys. Atom. Nucl. 2011. Vol. 74. P. 1615-1622.

2. Skobelev N.K., Penionzhkevich Yu.E., Voskoboinik E.I. et al. Fusion and Transfer Cross Sections of ^{3}He Induced Reaction on Pt and Au in Energy Range 10-24.5 MeV // Phys. Part. Nucl. Lett. 2014. Vol. 11. P. 208-215.

3. Wu Y., Ishikawa S., Sasakawa T. Three-Nucleon Bound States: Detailed Calculations of ^{3}H and ^{3}He // Few-Body Systems. 1993. Vol. 15. P. 145-188.

4. Dzhibuti R.I., Shitikova K.V. Metod gipersfericheskikh funktsiy v atomnoy i yadernoy fizike [Method of Hyperspherical Functions in Atomic and Nuclear Physics]. Moscow, Energoatomizdat, 1993. 269 P.

5. Kievsky A., Marcucci L.E., Rosati S. et al. High-Precision Calculation of the Triton Ground State Within the Hyperspherical-Harmonics Method // Few-Body Systems. 1997. Vol. 22. P. 1-10.

6. Viviani M., Kievsky A., Rosati S. Calculation of the α-Particle Ground State // Few-Body Systems. 1995. Vol. 18. P. 25-39.

7. Voronchev V.T., Krasnopolsky V.M., Kukulin V.I. A Variational Study of the Ground and Excited States of Light Nuclei in a Three-body Model on the Complete Basis. I. General Formalism // J. Phys. G. 1982. Vol. 8. P. 649-666.

8. Feynman R.P., Hibbs A.R. Quantum Mechanics and Path Integrals. New York, McGraw-Hill, 1965. 382 P.

9. Blokhintsev D.I. Osnovy kvantovoy mekhaniki [Principles of Quantum Mechanics]. Moscow, Nauka, 1976. 608 P.

10. Shuryak E.V., Zhirov O.V. Testing Monte Carlo Methods for Path Integrals in Some Quantum Mechanical Problems // Nucl. Phys. B. 1984. Vol. 242. P. 393-406.

11. Shuryak E.V. Stochastic Trajectory Generation by Computer // Sov. Phys. Usp. 1984. Vol. 27. P. 448-453.

12. Lobanov Yu.Yu. Functional Integrals for Nuclear Many-particle Systems // J. Phys. A: Math. Gen. 1996. Vol. 29. P. 6653-6669.

13. Lähde T.A., Epelbaum E., Krebs H. et al. Lattice Effective Field Theory for Medium-Mass Nuclei // Phys. Lett. B. 2014. Vol. 732. P. 110-115.

14. Borasoy B., Epelbaum E., Krebs H. et al. Lattice Simulations for Light Nuclei: Chiral Effective Field Theory at Leading Order // Eur. Phys. J. A. 2007. Vol. 31. 105-123.

15. Samarin V.V., Naumenko M.A. Study of Ground States of ^{3,4,6}He Nuclides by Feynman's Continual Integrals Method // Bull. Russ. Acad. Sci. Phys. 2016. Vol. 80, No. 3. P. 283-289.

16. NVIDIA CUDA. URL: `http://developer.nvidia.com/cuda-zone/` (accessed: 23.06.2016).

17. Sanders J., Kandrot E. CUDA by Example: An Introduction to General-Purpose GPU Programming. New York, Addison-Wesley, 2011. 290 P.

18. Perepyelkin E.E., Sadovnikov B.I., Inozemtseva N.G. Vychisleniya na graficheskikh protsessorakh (GPU) v zadachakh matematicheskoy i teoreticheskoy fiziki [Computing on Graphics Processors (GPU) in Mathematical and Theoretical Physics]. Moscow, LENAND, 2014. 176 P.

19. Ermakov S.M. Metod Monte-Karlo v vychislitel'noy matematike: vvodnyy kurs [Monte Carlo Method in Computational Mathematics. Introductory Course]. St. Petersburg, Nevskiy Dialekt, 2009. 192 P.

20. Pollyak Yu.G. Veroyatnostnoe modelirovanie na elektronnykh vychislitel'nykh mashinakh [Probabilistic Modeling on Electronic Computers]. Moscow, Sovetskoe Radio, 1971. 400 P.

21. Satcher G.R., Love W.G. Folding Model Potentials from Realistic Interaction for Heavy-Ion Scattering // Phys. Rep. 1979. Vol. 55, No. 3. P. 185-254.

22. Alvarez M.A.G., Chamon L.C., Pereira D. et al. Experimental Determination of the Ion-Ion Potential in the N=50 Target Region: A Tool to Probe Ground-State Nuclear Densities // Nucl. Phys. A. 1999. Vol. 656, No. 2. P. 187-208.

23. NRV Web Knowledge Base on Low-Energy Nuclear Physics. URL: `http://nrv.jinr.ru/` (accessed: 23.06.2016).

24. Heterogeneous Cluster of LIT, JINR. URL: `http://hybrilit.jinr.ru/` (accessed: 23.06.2016).